Available online at www.sciencedirect.com
SCIENCE DIRECT
Journal of Photochemistry and Photobiology A: Chemistry 180 (2006) 165–174
Journal of Photochemistry and Photobiology A:Chemistry
www.elsevier.com/locate/jphotochem

Photophysics of dibenzodioxocins

Antonio Eduardo da Hora Machado [a,*], Rodrigo De Paula [a], Reinaldo Ruggiero [a], Christian Gardrat [b], Alain Castellan [b]

[a] *Laboratório de Fotoquímica/GFQM, Instituto de Química, Universidade Federal de Uberlândia, P.O. Box 593, CEP 38400-902 Uberlândia, MG, Brazil*
[b] *Laboratoire de Chimie des Substances Végétales, Université Bordeaux I, F-33405 Talence, France*

Received 21 June 2005; received in revised form 11 October 2005; accepted 13 October 2005
Available online 14 November 2005

Abstract

The photophysics and photochemical reactivity of dibenzodioxocins (DBDO) was evaluated, considering experimental and theoretical data related to two model compounds, a phenolic and a non-phenolic and two theoretical analogues. Both compounds exhibit similar photophysical properties, influenced by solvent polarity.

Expressive quantum yields of intersystem crossing were observed for both compounds, in aprotic and non-polar medium and in protic and considerably polar medium, being sensitive to solvent polarity—presenting a small decrease as solvent polarity increases, whereas Φ_F presents inverse trend. A competition between fluorescence and intersystem crossing governs the deactivation of the excited state, being favourable for the last.

The photooxidation of these compounds must occur by a complex mechanism, involving the free radicals formed in the S_1 state, due to α–O–4 and β–O–4 bond cleavage, rearranged products and molecular oxygen in parallel and secondary reactions.

Evidences are presented about the participation of singlet oxygen sensitized from the triplet state of these compounds. The non-phenolic compound is the most reactive, with $\Phi_R = 0.37$.

Theoretical data suggest that the lowest reactivity of the phenolic DBDO ($\Phi_R = 0.16$) is due to the presence of the hydroxyl group in the 4 position of the phenyl group. The strong electron donor character strengthens the β–O–4 bond, inducing some reversibility of the α–O–4 bond cleavage, confirming a proposal previously made by Castellan and co-workers, based on the analysis of experimental data.

Keywords: Photophysics; Photooxidation; Dibenzodioxocins; Singlet oxygen; B3LYP; SAM1

1. Introduction

Dibenzodioxocins (DBDO) are a class of wood components, mainly softwood, which exert an important role in the degradation of lignocellulosics [1]. The presence of both photoreactive α–O–4 and β–O–4 linkages brings a high photosensitivity to its framework. The importance of DBDO in lignin degradation is related to the relatively high abundance of biphenyl groups in its structure [2–4].

In previous works, some of us have verified, based on experimental evidences, that under oxygenation non-phenolic DBDO suffers efficient UV-A induced decomposition, resulting in stilbenoid and biphenilic compounds as intermediates and a series of colored photoactive products, whereas its phenolic analogue showed to be less reactive [1,5]. Based on products analysis, a free radical mechanism was proposed for the primary steps of the DBDO photooxidation, involving an α–O–4, followed by β–O–4 bond cleavage [1]. Secondary reactions, involving molecular oxygen or rearrangements, were proposed as being responsible by the formation of oligomeric and oxidized fragments [1]. Despite this, the difference of reactivity between phenolic and non-phenolic DBDO was not still well clarified. Besides, photophysical data about this class of compounds is practically non-existent.

In the present work, evidences are presented, founded in data from quantum mechanical calculations and in the analysis of photophysical, photochemical and spectroscopic data obtained for two DBDO model compounds and opti-

* Corresponding author. Fax: +55 34 3239 4208.
E-mail address: aeduardo@ufu.br (A.E.H. Machado).

1010-6030/$ – see front matter © 2005 Elsevier B.V. All rights reserved.
doi:10.1016/j.jphotochem.2005.10.011

mized analogues, which add new facts to the proposed mechanism.

2. Experimental

The compounds 6-(4-ethoxy-3-methoxyphenyl)-4,9-dimethoxy-2,11-di-*n*-propyl-6,7-dihydro-5,8-dioxa-dibenzo [*a*,*c*] cyclooctene (DBDO 1) and 6-(4-hydroxy-3-methoxyphenyl)-4,9-dimethoxy-2,11-di-*n*-propyl-6,7-dihydro-5,8 dioxa-dibenzo [*a*,*c*] cyclooctene (DBDO 2), respectively, non-phenolic and a phenolic DBDO models (Fig. 1), were synthesized in the Laboratoire de Chimie des Substances Végétales, UB1 [1]. In this work, their spectroscopic and photophysical behaviour were investigated in ethanol, 1-octanol, 1,4-dioxane and methyl-cyclohexane (MCH).

The compounds **3** and **4** are simplified DBDO structures, representing, respectively, the phenolic and non-phenolic forms, idealized to be used as models for quantum mechanical calculations, aiming to reduce the computational effort.

UV–vis absorption, excitation and emission spectra were recorded using, respectively, a Shimadzu UV-2501 PC spectrophotometer and a HITACHI F-4500 spectrofluorimeter equipped with accessories for low-temperature measurements, being the fluorescence spectra obtained using right angle configuration.

Fluorescence measurements at 298 K were done for the solutions containing the DBDO models in all studied solvents. Measurements at 77 K were done for previously deoxygenated solutions prepared in methylcyclohexane and ethanol. Argon was used to deoxygenate these solutions. For these measurements, the solutions were prepared with absorbance lower than 0.100 at the excitation wavelength to avoid light reabsorption effects. The emission and excitation slits were of 2.5 mm. The xenon lamp was operated at 950 V and the scanning rate adjusted to 240 nm min^{-1}.

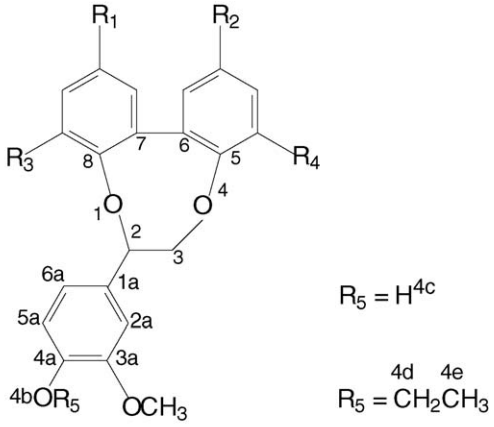

1) $R_1 = R_2 =$ n (C_3H_9); $R_3 = R_4 = OCH_3$; $R_5 = CH_3CH_2$
2) $R_1 = R_2 =$ n (C_3H_9); $R_3 = R_4 = OCH_3$; $R_5 = H$
3) $R_1 = R_2 = H$; $R_3 = R_4 = CH_3$; $R_5 = CH_3CH_2$
4) $R_1 = R_2 = H$; $R_3 = R_4 = CH_3$; $R_5 = H$

Fig. 1. Representation of the compounds involved in the study: (**1**) 6-(4-ethoxy-3-methoxyphenyl) -4,9-dimethoxy-2,11-di-*n*-propyl-6,7-dihydro-5,8-dioxa-dibenzo [*a*,*c*] cyclooctene; (**2**) 6-(4-hydroxy-3-methoxyphenyl)-4,9-dimethoxy-2,11-di-*n*-propyl-6,7-dihydro-5,8-dioxa-dibenzo [*a*,*c*] cyclooctene; (**3**) 6-(4-ethoxy-3-methoxyphenyl)-4,9-dimethyl-6,7-dihydro-5,8-dioxa-dibenzo [*a*,*c*] cyclooctene; (**4**) 6-(4-hydroxy-3-methoxyphenyl)-4,9-dimethyl-6,7-dihydro-5,8-dioxa-dibenzo [*a*,*c*] cyclooctene. The numbering over part of the structure is related to discussion of Table 3.

The fluorescence quantum yields were estimated from the corrected fluorescence spectra, using the secondary standard methodology, proposed by Eaton [6]. Naphthalene, in cyclohexane ($\Phi_F = 0.23$ at 298 K) was selected as standard for these measurements.

Time-resolved fluorescence measurements were performed for solutions prepared in ethanol using a CD 900 fluorescence lifetime spectrometer, from Edinburgh Analytical Instruments. The time profile of the exciting pulse (a hydrogen-filled flash lamp operating at 40 kHz) was recorded under the same conditions by replacing the sample with a scattering solution (colloidal silica). It was compared to the experimental fluorescence decay profile, furnishing the time profile of the sample [7,8]. These measurements were done without the use of lifetime standards. For data analysis, the software of the equipment was used. These experiments were done using a time base of 100 ns and 5000 counts in the maximum channel.

3. Kinetic measurements

DBDO solutions ($\approx 10^{-4}$ mol dm^{-3}) were prepared in hydrated ethanol (approximately 20% water) and photolysed in quartz cuvettes, at room temperature, under aeration and constant stirring, using monochromatic radiation ($\lambda = 280$ nm), furnished by a 400 W high-pressure mercury lamp. The incident radiation was selected by the use of a monochromator (ISS, with 100 mm focal distance). To confirm whether the reactions involves the participation of singlet oxygen, the photolysis were done in the absence and presence of sodium azide (between 0.4×10^{-5} and 1.5×10^{-5} mol dm^{-3}), a known physical quencher of singlet oxygen [9]. The absorption spectra of the photolysed solutions were recorded at different times of photolysis, in a range between 200 and 320 nm. These experiments were complemented by HPLC measurements (Shimadzu LC10AD and SPD-10A, UV detection at 280 nm), using methanol/water 70:30 as eluent, with a flow rate of 1 mL min^{-1}. By the ratio of areas at different times of irradiation, the percentage of conversion and the reaction quantum yield, Φ_R, for the degradation in the presence or not of sodium azide, could be estimated. The photonic flux at 280 nm furnished by the lamp was measured using the setup mounted for the kinetic experiments and a previously calibrated radiometer built using optical items furnished by Ocean Optics. The value found is equal to 9.62×10^{13} photons s^{-1} (1.60×10^{-10} einstein s^{-1}).

4. Quantum mechanical calculations

The reaction paths for the cleavage of the α–O–4 and β–O–4 bonds were calculated for ground and excited state for both analogues (compounds **3** and **4**), using the Semi-Ab Initio Method,

Version 1 (SAM1) method [10]. For reaction paths in the excited state, the first singlet excited state was optimized using complete active space–configuration interaction (CAS–CI) methodology, in a quadratically convergent SCF calculation. The optimizations were done following the energy, using the keyword TRUST. The active space was generated using a subset of two CI active molecular orbitals (CI = 2) from 44 states available. From this procedure, four microstates were kept. The CI active MOs were based on Bracket Fermi Level. The reaction path calculations were performed also using CAS–CI, under the same conditions used in the optimization. These calculations were implemented using AMPAC 8.16.1 program suite [10].

The activation barriers for the studied processes were approximately estimated considering $E_a \approx \Delta^{\#}H^{\circ}$ [11].

The S_0 state structure optimization was done using density functional theory, taking as start point the SAM1 ground state structure. The B3LYP hybrid functional [12] and the 6-31G* basis set were used for these optimizations. The structure of S_1 and T_1 were optimized using the CIS approach and were used to calculate the excitation energies and oscillator strengths using the time-dependent extension of the density functional theory [13].

The excitation energies and corresponding oscillator strengths were calculated using TD-DFT with the same hybrid functional [14] and the 6-31G** basis set, for singlet–singlet and *compact effective potentials* (CEP)-4G* for singlet–triplet transitions. These calculations were implemented using the Gaussian 03W program suite [13]. All theoretical data were obtained only for isolated structures.

5. Results and discussion

5.1. Spectroscopic analysis

Fig. 2 presents UV–vis absorption spectra of DBDO 1 and 2 in ethanol.

These spectra are very similar for both compounds. The non-structured shape remembers a lignin-like absorption spectrum [15]. The peak at 220 nm is characteristic of the conjugate transition of aromatic groups. A shoulder at 254 nm, is probably the result of the overlap between conjugate and benzenoid π,π^* transitions. Finally, the low-intensity band, in the range between 270 and 300 nm, with peak centred at about 284.5 nm (4.36 eV), attributed to the $S_0 \rightarrow S_1$ transition, involves a benzenoid π,π^* transition, based on biphenyl group, confirmed by the analysis of molecular orbitals. For both compounds, the estimated log ε for this peak is between 3.6 and 3.8 in all studied solvents (Table 1), being usually slightly higher for phenolic DBDO. Considering the value of log ε and the small value of the oscillator strength (0.0597) estimated from theoretical calculation, this transition can be considered as being at the inferior limit of the range of molar absorptivities attributed to "fully allowed" transitions [16,17]. This is probably due to the steric disposition between the aromatic rings of the S_0 state (the dihedral angle is equal to 48.98°, Fig. 3), which must compromise partially the overlap between the orbitals involved in the transition [16,18] and the small energy difference between S_1 and S_2 states (as verified by TD-DFT calculations, in a range between 0.7 and 1.0 eV), resulting in a mixed state with a partial n,π^* character due to the participation of the S_2 state ($\Phi = \phi(S_1) + \lambda\phi(S_1)$, where $0 < \lambda < 1$).

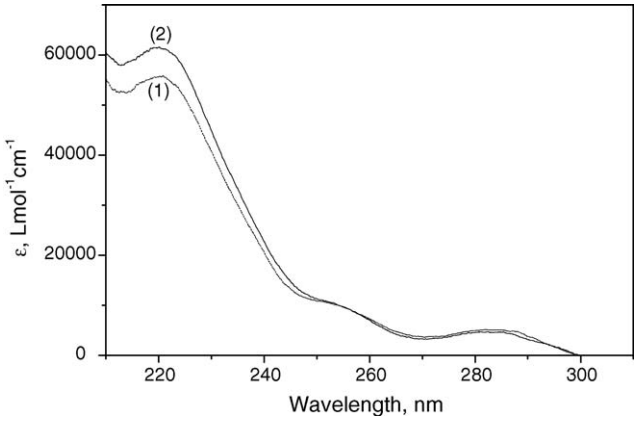

Fig. 2. Absorption spectra of compounds **1** (5.7×10^{-6} mol dm^{-3}) and **2** (5.7×10^{-6} mol dm^{-3}), in ethanol solution.

Both states present the same symmetry (C_1). Only a small difference is expected in the dihedral angle between the aromatic rings of the biphenyl group, based on the theoretical data (48.98° for S_0 and 53.82° for S_1). For biphenyl, the dihedral angle measured by X-ray diffraction is equal to $44.4 \pm 1.2°$ [19,20].

The excitation energy for this transition calculated using a TD-DFT methodology (4.72 eV; 263.05 nm), shows a good agreement with the experimental data, being 0.35 eV (8%) higher than the energy of the peak centred at 284.0 nm. This good agreement is in accordance with the reported about TD-DFT data for excitation energies of low lying excited states. The expected results, mainly using the B3LYP hybrid functional, are accurate, being usually some tenths of eV high [12,21–24]. Besides, B3LYP hybrid functional typically gives the correct ordering of states [12].

5.2. Photophysics

Table 1 brings the available photophysical data for DBDO 1 and 2.

Using the $E_T(30)$ empirical solvatochromic scale [25,26] to express polarity, it was observed a very small change in the absorption λ_{max} corresponding to the $S_0 \rightarrow S_1$ transition as solvent polarity varies. On the other hand, the excited state is very sensitive to these changes, confirming that $S_0 \rightarrow S_1$ corresponds to a π,π^* transition. The values of Stokes' shift are very expressive, varying between 5271 and 6146 cm^{-1} for both compounds, increasing as solvent polarity increases. The very small energy difference between S_1 and S_2 explains the effect on the absorption λ_{max}.

For the emission spectra, as solvent polarity increases, the energy difference between these states tends to increase since, under this condition, S_1 due to its π,π^* character is better solvated. As consequence, the n,π^* character of the mixed state will decrease and an increasing bathofluoric shift and Φ_F will

Table 1
Photophysical data for compounds **1** and **2**, obtained under different solvents

Solvent	$E_T(30)$ (kcal mol^{-1}) [25]	λ_{max} (abs) (nm)		log ε		Stokes' shift (cm^{-1})		Φ_F at 298 K (77 K)		Φ_{IC} (Φ_{ISC})		Calculated τ_F^0 (ns)	
		DBDO 1	DBDO 2	DBDO 1	DBDO 2	DBDO 1	DBDO 2	DBDO 1 (±0.02)	DBDO 2 (±0.02)	DBDO 1	DBDO 2	DBDO 1 (±2)	DBDO 2 (±2)
MCH	31.0	284.0	284.0	3.617	3.712	5271	5361	0.09 (0.21)	0.11 (0.15)	0.12 ± 0.02 (0.79 ± 0.14)	0.04 ± 0.01 (0.85 ± 0.15)	9.7	8.4
1,4-Dioxane	36.0	284.0	284.3	3.787	3.829	6108	6071	0.15	0.15	–	–	13.5	12.7
1-Octanol	48.1	281.0	284.3	3.747	3.799	6141	5789	0.16	0.15	–	–	8.4	7.5
Ethanol	51.9	284.0	284.1	3.716	3.739	6125	6146	0.16 (0.22)	0.14 (0.20)	0.06 ± 0.01 (0.78 ± 0.14)	0.06 ± 0.01 (0.80 ± 0.14)	17.8	15.1

MCH: methyl-cyclohexane; the τ_F (1.02 ± 0.01 for DBDO 1 and 0.95 ± 0.01 for DBDO 2) were also used to calculate the rate constants and quantum yields for MCH.

be observed. Although sounds premature due to the number of solvents in the set, the collected data suggest that these shifts tend to present an expressive increase in aprotic solvents, as solvent polarity increases, whereas between protic solvents a small but positive variation must be observed. This small variation in the Stokes' shift in the group of protic solvents is probably due to the small changes in the intensity of the strong and specific polar interactions, as solvent polarity varies. However, very expressive changes must be observed for this class of solvents when compared to non-polar solvents.

Despite its capability to form hydrogen bonding, 1-octanol was considered in both groups, since it has some characteristics of non-polar solvent due to its long carbonic chain. We have observed a similar behaviour in a study on the photophysics of zinc phthalocyanine [27].

About 1,4-dioxane, despite it presents a trend to suffer anomalous behaviour, being sometimes a non-polar or a 'pseudo-polar' solvent [26], its behaviour is, in this case, characteristic of a polar one.

Considering that at 298 K, $\Phi_F + \Phi_{IC} + \Phi_{ISC} = 1$ and that at 77 K, $\Phi_F + \Phi_{ISC} = 1$, the quantum yields of intersystem crossing (Φ_{ISC}) and internal conversion (Φ_{IC}) could be estimated (Table 1). The Φ_F in MCH is the lowest for both DBDO in the set of solvents. This occurs due to the non-polar character of this solvent, in which the energy difference between S_1 and S_2 must assume the lowest value in the set.

The quantum yields of intersystem crossing assumes expressive values, much higher than Φ_F and Φ_{IC}, insinuating a predominance of intersystem crossing as deactivation route of the excited state. Thus, we can consider $\frac{\Phi_F}{\Phi_{ISC}} \equiv \frac{k_F}{k_{ISC}} \ll 1$.The value of Φ_{ISC} is affected by the solvent polarity. A numeric exercise shows that k_{ISC} is approximately nine times faster than k_F for DBDO 1 in MCH and almost five times faster, in ethanol. In other words, as $\Delta E(S_1,S_2)$ increases, favouring Φ_F, the quantum yield of intersystem crossing decreases. Similar behaviour is observed for DBDO 2.

The Φ_{IC} is considerably small for all solvents, most probably due to the large value of $\Delta E(S_1,S_0)$ [17] and the relative rigidity of these molecules.

The natural lifetime was estimated from,

$$\tau_F^0 = \frac{\tau_{exp}}{\Phi_F} \quad (1)$$

where τ_{exp} is the measured lifetime estimated from TCSPC measurements.

These data could be compared to the natural lifetime calculated from the absorption spectra [17],

$$\tau_F^0 = \frac{3.417 \times 10^8}{(\tilde{\nu})^2_{max} n^2 A} \quad (2)$$

where $A = \int \varepsilon(\tilde{\nu}) d\tilde{\nu}$; n is the solvent refractive index; $(\tilde{\nu})^2_{max}$ is the wavenumber of the transition in the absorption maximum.

The natural lifetimes based on the absorption spectra (Eq. (2)) for the solutions prepared in methyl-cyclohexane, respectively, 9.7 ns ($k_F^0 = 1.03 \times 10^8\ s^{-1}$) and 8.4 ns ($k_F^0 = 1.19 \times 10^8\ s^{-1}$) for DBDO 1 and 2, show good agreement with the estimated

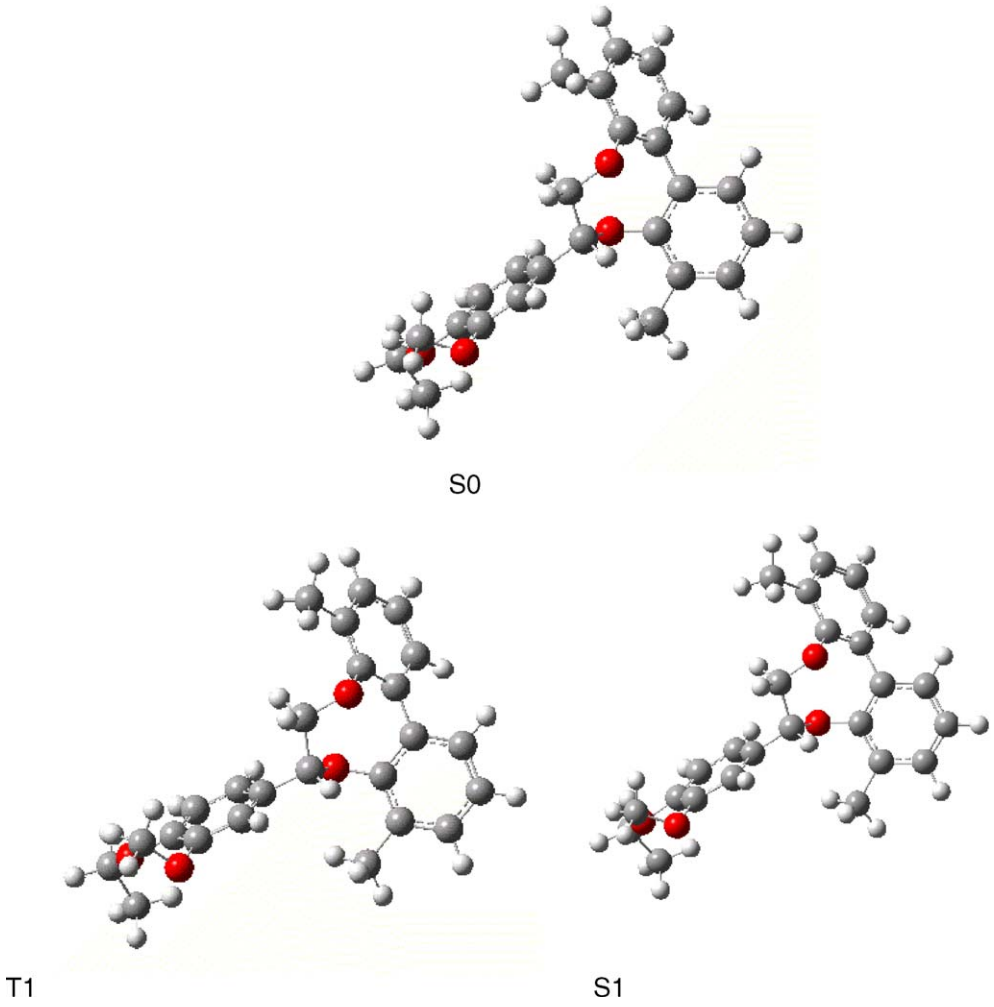

Fig. 3. Representation of the optimized structure for S_0, S_1 and T_1 states, for a non-phenolic DBDO analogue (compound **3**). All species have C_1 symmetry. The calculated torsion angle between rings in the biphenyl group is equal to 48.98° for S_0, 53.82° for S_1 and 44.76° for T_1.

for the solutions in methyl-cyclohexane using the measured lifetimes and assuming that the τ_{exp} measured in ethanol is also equivalent in this solvent. The values for τ_F^0 are, respectively, 11.3 ns ($k_F^0 = 8.85 \times 10^7\ s^{-1}$) and 8.6 ns ($k_F^0 = 1.16 \times 10^8\ s^{-1}$).

In ethanol, the τ_F^0 calculated from Eq. (2) (17.8 ns for DBDO 1 and 15.1 ns for DBDO 2) does not show agreement with the ones estimated from the measured lifetimes, 6.38 ns ($k_F^0 = 1.57 \times 10^8\ s^{-1}$) and 6.79 ns ($k_F^0 = 1.47 \times 10^8\ s^{-1}$), respectively, for DBDO 1 and 2. This shortening is certainly the result of the better relaxation of the S_1 state in protic solvents, which Eq. (2) is incapable to depict. From the measured lifetimes in ethanol, the fluorescence rate constants were estimated as being, respectively, $k_F = 9.80 \times 10^8\ s^{-1}$ for DBDO 1 and $1.05 \times 10^9\ s^{-1}$ for DBDO 2. These rate constants are, respectively, six and seven times faster than the natural decay calculated from Eq. (2).

The data of fluorescence lifetime suggest monoexponential decay for both compounds, with a fluorescence lifetime around 1 ns, probably related to the biphenyl structures. In a previous work involving the characterization of lignins in solution, using fluorescent probes [29], we observed a bimodal profile for the lifetime distribution of lignin fragments obtained from *E. Grandis* wood. The analysis of the histogram indicated the presence of at least two important groups of fluorophores in this kind of lignin, being the first peak with a lifetime between 1.33 ± 0.21 and 1.36 ± 0.17 ns, with a relative weight above 80%, most probably related to different biphenyl structures. Castellan et al. has reported a lifetime of 1.6 ns for a phenolic biphenyl lignin model in methanol solution [30].

As 1-octanol is a relatively viscous solvent (10.6 cp at 288 K), possessing a long carbon chain and a hydroxyl group, it could be considered as an approximate model to anticipate the photophysical behaviour of a DBDO physically associated (adsorbed) to cellulose fibres. Concerning to the behaviour of DBDO in lignocellulosics, this subject needs to be carefully treated considering, in this case, the large number of variables involved, like as different microenvironments, changes of conformation, specific interactions involving lignin fragments, etc. [29,30]. For example, the rigidity of the medium is capable to induce shortening in the τ_{exp} of the fluorophore. Castellan et al. have observed this for a set of lignin models adsorbed in cellulose [30].

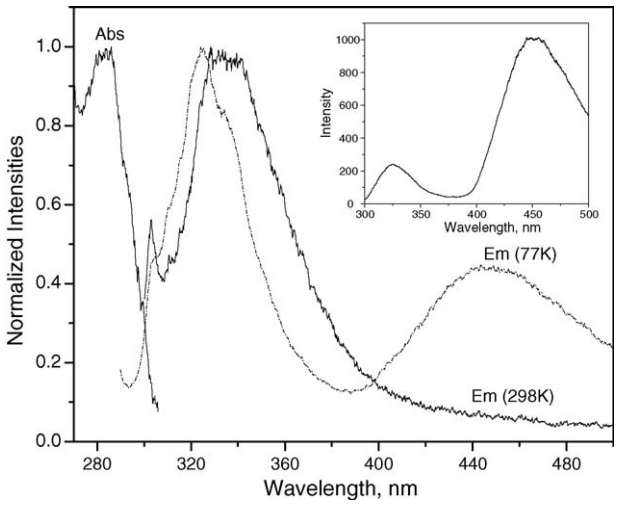

Fig. 4. Superposition between the emission spectra of DBDO 2, in methylcyclohexane, at 77 and 298 K and the absorption spectrum at 298 K. The band attributed to phosphorescence (λ_{exc} = 277 nm, λ_{em} = 446 nm) can be observed in the emission spectrum at 77 K. *Inset:* emission spectrum in ethanol, at 77 K (the phosphorescence λ_{em} occurs at 451 nm).

5.2.1. State energies

Fig. 4 presents the superposition between absorption and fluorescence spectra obtained for DBDO 2, in methylcyclohexane at 77 and 298 K.

The singlet energies for DBDO 1 and 2 were estimated from the crossing of the normalized absorption spectra. In the studied solvents, since emission spectra at 77 K do not show vibrational structure. The values show a minimal difference between both compounds, respectively, 4.40 eV (282 nm) and 4.34 eV (285 nm) and a small difference when compared to the value estimated for the biphenyl, 4.33 eV (286.5 nm) [28].

An expressive phosphorescence band can be seen for these compounds, as in MCH as in ethanol, for the deoxygenated solutions at 77 K. Due to the shape of the phosphorescence spectra (Fig. 4), the triplet energy could not be self-confidently estimated from experimental data. Although, a theoretical estimate of this energy furnishes a value equal to 3.17 eV (391.5 nm) for $E(T_{1\text{-}0})$, acceptable considering the profile of the phosphorescence band. The prediction of the ordering and energies of the triplet states were done using the CEP-4G* basis set, which gave the most acceptable results in this case, since time-dependent calculations for singlet–triplet excitation energies using *compact effective potentials* basis set furnished a more consistent value for T_1 energy, taking as reference the profile of phosphorescence spectrum. The TD-DFT calculations also reveal a considerable density of triplet states, with nine triplet states with energy lower than $E(S_1)$ for these compounds.

The large values of Φ_{ISC} can be attributed to the low energy gap between S_1 and T_9 and to the high density of triplet states between S_1 and T_1, as suggested by TD-DFT calculations. The estimated energy gap between S_1 and T_9, 0.13 eV (12.5 kJ mol^{-1}), is sufficiently small to justify a favourable Franck–Condon factor [17], allowing an efficient population of the triplet state for both compounds.

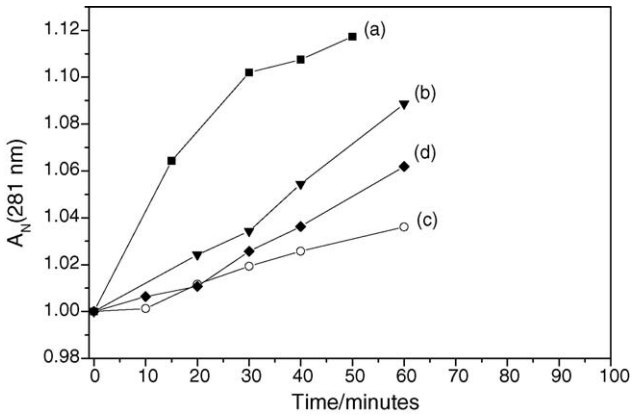

Fig. 5. Normalized absorbance at 281 nm vs. time of photolysis for the photooxidation of DBDO 1 and 2, in the presence or not of sodium azide: (a) DBDO 1; (b) DBDO 2; (c) DBDO 1/N_3^-; (d) DBDO 2/N_3^-. The reactions were done with monochromatic radiation (281 nm), for aerated ethanol solutions.

On the other hand, the expressive values of Φ_{ISC} and the energy magnitude of T_1, despite τ_T is still unknown, suggest the possibility of singlet oxygen sensitization and consequently its participation in the photooxidation of these compounds.

5.3. On the participation of singlet oxygen during DBDO photooxidation

As the participation of singlet oxygen is a possibility, as evidenced previously, kinetic evaluations of the photooxidation of DBDO 1 and 2 were done in aerated solutions, in the presence or not of sodium azide, a known singlet oxygen quencher [9]. By the magnitude of the quenching constant (in ethanol, between 2.0×10^8 and 3.9×10^8 dm^3 mol s^{-1}), this process is based on a charge transfer reaction between $^1O_2$ and N_3^- [9,31].

Fig. 5 presents the observed changes in the absorbance of both DBDO at 281 nm, during the photolysis, using monochromatic light (281 nm).

As can be observed, the non-phenolic compound (DBDO 1) is the most reactive and susceptible to the action of $^1O_2$. However, the incorporation of NaN_3 to the solutions was not capable to suppress completely the reaction (Table 2), suggesting that singlet oxygen is not the main agent in the degradation of these compounds. The maximum suppression implied in a reduction of less than 30% in Φ_R for DBDO 1. For DBDO 2,

Table 2
Percentage of conversion and quantum yield (Φ_R) for the degradation of the compounds **1** and **2** in ethanol, with and without sodium azide, after 60 min of reaction, estimated by HPLC measurements

Compound	% Conversion (±10%)		Φ_R[b]	
	Without NaN_3	With NaN_3	Without NaN_3	With NaN_3
1	27[a]	35	0.37	0.26
2	35	36	0.16	0.15

[a] The data for DBDO 1 were estimated after 30 min of reaction, due to its highest rate of conversion.

[b] The Φ_R is based on the photonic flux of the incident light, during the photolysis.

Table 3
Mulliken's net atomic charges before and after α—O—4 bond cleavage in the S_1 state and for the non-cleaved compounds in the ground state

Atom	Number	Phenolic			Non-phenolic		
		Before		After	Before		After
		S_0	S_1	S_1	S_0	S_1	S_1
O	1	−0.295	−0.212	−0.481	−0.294	−0.209	−0.464
C	2	0.077	0.076	−0.116	0.085	0.082	−0.145
C	3	−0.064	−0.054	−0.082	−0.066	−0.055	−0.064
O	4	−0.298	−0.229	−0.269	−0.299	−0.229	−0.267
C	5	0.104	0.165	0.062	0.105	0.164	0.062
C	6	–	−0.002	0.054	–	−0.001	0.057
C	7	–	−0.015	−0.097	–	−0.017	−0.093
C	8	0.104	0.137	0.288	0.104	0.137	0.291
C	1a	−0.043	−0.036	−0.102	−0.048	−0.041	−0.098
C	2a	0.171	−0.175	−0.181	−0.172	−0.176	−0.169
C	3a	0.095	0.103	0.102	0.087	0.093	0.074
C	4a	0.063	0.076	0.105	0.070	0.084	0.131
O	4b	−0.351	−0.352	−0.315	−0.284	−0.282	−0.234
H	4c	–	0.227	0.248	–	–	–
C	4d	–	–	–	−0.067	−0.067	−0.074
C	4e	–	–	–	−0.357	−0.357	−0.362
C	5a	−0.203	−0.206	−0.243	−0.202	−0.203	−0.235
C	6a	−0.160	−0.154	−0.107	−0.161	−0.154	−0.152

The used numbering to describe the atoms is presented in Fig. 1.

most probably due to its inertia to suffer oxidation, the presented information is not conclusive about the participation of singlet oxygen on these reactions. Castellan and co-workers justified the low reactivity of the phenolic DBDO to the presence of the phenolic group in the 4 position of phenyl ring, based on data from mass spectrometry, which suggest the reversible formation of an intermediate quinone-methide after α–O–4 bond cleavage [5].

In Table 2, the percentage of conversion and Φ_R for the photooxidation of both compounds, are presented. For DBDO 1 without sodium azide, the percentage of conversion was calculated considering 30 min of reaction, since this compound presents the higher degradation rate. The other data are all related to 60 min of reaction.

By steric reasons and analysing the charge distribution over these molecules in the ground state (Table 3), the chances to occur a direct attack of $^1O_2$ over the bond between the α carbon and the phenyl ring, the most feasible region for an attack like this, are minimal. On the other hand, if this attack occurs after the homolytic cleavage of α–O–4 bond, it is completely viable (Table 3).

The Φ_R found for DBDO 1 in the absence of sodium azide is identical to the value reported by Castellan and co-workers [1], whereas the data for DBDO 2 is more than ten times high the value proposed for the reaction occurring in methanol [5].

5.4. Theoretical simulation of the first steps of the DBDO degradation

The asymmetry between absorption and emission spectra (Figs. 2 and 4), evidencing the occurrence of chemical reaction in the excited state [7], previous experimental data [1,5] and the secondary influence of $^1O_2$ on the degradation of these compounds, suggest that the photochemical degradation of DBDO must begin with the homolytic cleavage of α–O–4 and β–O–4 bonds in the S_1 state, as previously suggested [1,5], since these bonds are admittedly very photoactive [32,33].

Table 4
Activation energies (kJ mol^{-1}) for the two step photodegradation of DBDO, calculated using SAM1

DBDO	α Cleavage	β Cleavage
Non-phenolic	70.8	89.7
Phenolic	71.5	98.7

The analysis of the activation barriers from the reaction paths for α–O–4 and β–O–4 bond cleavages confirms that these bond ruptures will occur efficiently in the S_1 state (Table 4), being the α–O–4 bond cleavage the former, since it requires less energy to occur (Fig. 6).

The theoretical data suggest that the phenolic model is less able to suffer photooxidation, as proposed by Castellan and co-workers [5]. As show the results, the hydroxyl group in the 4-position of the phenyl ring (Fig. 1) increases the electron density in the region of β–O–4 bond, inducing its strengthen, implying in a higher activation barrier for the cleavage of the β–O–4 bond (Table 4), which induces the reversibility of the α–O–4 bond cleavage. This agrees with the experimentally observed, based on the analysis of mass spectra [5].

The β–O–4 bond strengthening can be observed by the analysis of the molecular potential energy surface superimposed onto total electron density, after the α–O–4 bond cleavage of the phenolic model (figure not shown). For the non-phenolic DBDO, being the ethoxyl group a moderately activating group, its action is not capable to strength the β–O–4 bond, which favours its photodegradation.

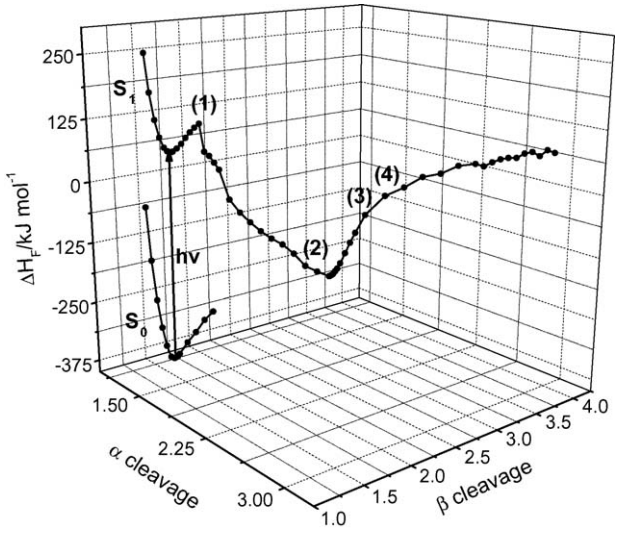

Fig. 6. Representation of the reaction coordinate containing the first stages of the oxidative photodegradation mechanism for non-phenolic dibenzodioxocins: (1) α—O—4 bond cleavage; (2) relaxed biradical; (3) β—O—4 bond cleavage; (4) excited stilbenoid and biphenylic compounds.

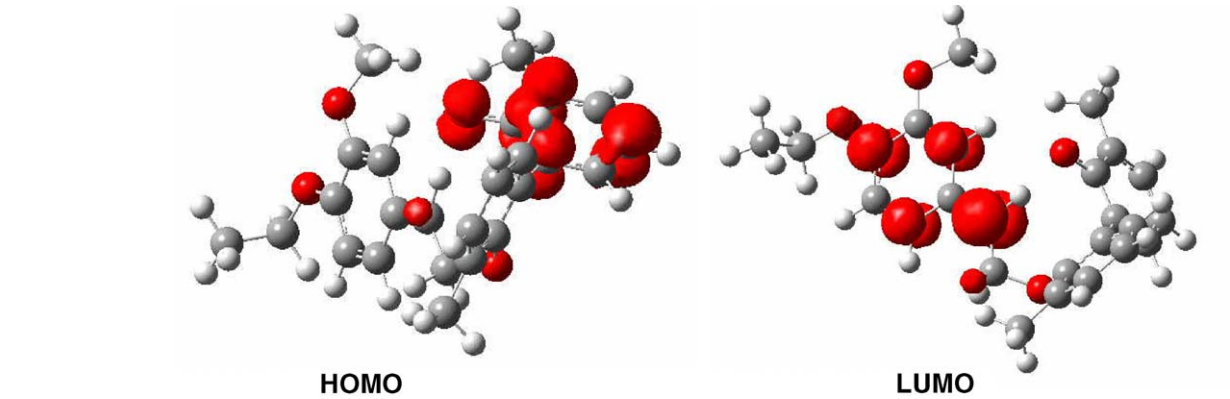

Fig. 7. Spin density isosurface for 6-(4-ethoxy-3-methoxyphenyl)-4,9-dimethyl-6,7-dihydro-5,8-dioxa-dibenzo [*a*,*c*] cyclooctene (compound **3**) after α—O—4 bond cleavage.

The analysis of Mulliken's net atomic charges shows for the phenolic DBDO, after α–O–4 bond cleavage, a considerable increase in the electronic density between the β–O–4 bond and the phenyl ring (Table 3 and Fig. 1), due to the strong electron donor character of hydroxyl group. After α–O–4 bond cleavage, the residual negative charge over the carbon atom (C1a) in opposition to the functional group in the 4 position of the phenyl ring increases more than 83% for phenolic DBDO, resulting in a bond with the α carbon (C2, Fig. 1) with an almost double bond character, as suggested by the formation of a quinone-methide intermediate, in previous work [5]. For the non-phenolic one the residual negative charge increases around 39%.

An increase of 52 and 18% in the electronic charge is also observed, respectively, over β carbon (C3) and the adjacent oxygen (O4). For non-phenolic DBDO, these changes are lower, respectively, 16 and 17% (Table 3).

The spin density isosurfaces, calculated for the biradical formed after α–O–4 bond cleavage, confirms that these cleavages follow a free radical mechanism. Fig. 7 presents the spin density isosurface for the non-phenolic model (compound **3**).

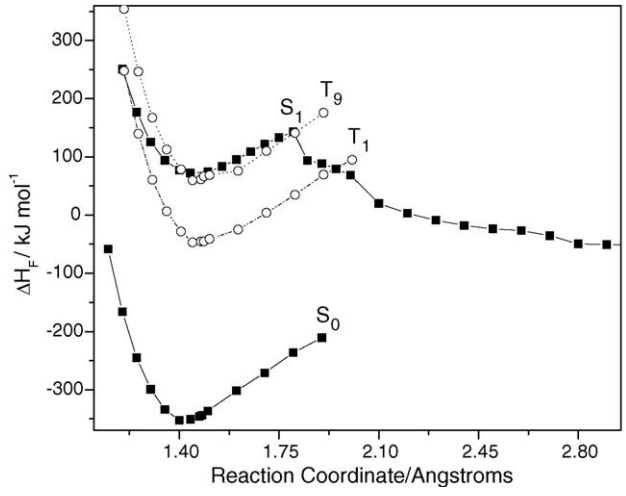

Fig. 8. Representation of the potential energy curves for S_0, S_1, T_1 and T_9 for the non-phenolic model.

The non-zero spin density (clouds over the atoms) occurs on oxygen (O1, Fig. 1) and the adjacent aromatic ring from biphenyl structure, for HOMO and on α carbon (C2) and phenyl ring, for LUMO, due to the electron delocalization, which stabilizes the biradical. This agrees with the expected for open-shell molecules, where non-zero spin density is an indication of occurrence of unpaired electrons [34].

Fig. 8 shows a representation of the potential energy surfaces (PES) for the non-phenolic model (compound **3**), related to S_0, S_1, T_1 and T_9. The surfaces for triplet states were built considering their relative positions due to the energy gap between them and S_1. As can be seen, T_9 crosses S_1 PES in two points, whereas T_1 crosses the surface at a point in the surface related to the biradical. These cross points confirm the efficient intersystem crossing observed for these compounds.

6. Conclusions

The combination of theoretical and experimental data furnished relevant information on the behaviour of DBDO who confirm a proposition made in previous works on the photooxidation mechanism and reactivity of this class of compounds and introduced a new insight about this process. The results suggest that the photooxidation of these compounds is based in a complex mechanism, which involves a two-step homolytic bond cleavage (α–O–4 and β–O–4 bonds) in the S_1 state and parallel and secondary reactions involving molecular oxygen ($^3O_2$ and $^1O_2$), the radicals from α–O–4 or from both cleavages and rearranged products, like as stilbenoid and biphenyl oxidized (quinone type) structures.

The experimental data suggest similar photophysical behaviour for both models, with considerably low fluorescence lifetime and a competition between fluorescence and intersystem crossing, favourable for this last process, as routes for deactivation of the excited state. The Φ_{IC} is usually low for both compounds. The value of Φ_F seems to be solvent-dependent, with a trend to increase as solvent polarity increases, whereas Φ_{ISC} does not change significantly as solvent polarity varies.

The S_1 state is related to a benzenoid transition involving the biphenyl group.

The population of the triplet state is a very efficient process, justified by the small energy gap between S_1 and the adjacent triplet state (12.5 kJ mol^{-1}) and the high density of triplet states between S_1 and T_1. Theoretical data show that the potential energy curve corresponding to S_1 state must be crossed in several points by the curves of T_9, adjacent to S_1 and T_1, which shows by another perspective the efficient population of the T_1 state.

The efficient population of the triplet state and its state energy, suggest that it is able to generate singlet oxygen by photosensitization.

The analysis of DBDO photooxidation confirms the participation of singlet oxygen in the photooxidation of these compounds. However, singlet oxygen exerts a secondary role on these reactions.

A re-evaluation of Φ_R for both compounds confirms the better reactivity of the non-phenolic DBDO and the value previously estimated in aerated benzene. However, although the low reactivity of the phenolic DBDO has been confirmed, the Φ_R estimated for its degradation is about ten times higher than the previous value.

The analysis of Mulliken's net atomic charges show that the minor reactivity presented by the phenolic DBDO is due to the strong electron donor character of the hydroxyl group in the 4 position of phenyl ring, which is capable to induce some reversibility on α–O–4 bond cleavage.

The theoretical methods applied in this work furnished very useful informations on the photophysics and aspects of DBDO chemical reactivity. Particularly, SAM1 (CAS–CI) showed to be able to give useful and reliable data on the S_1 state of these compounds. The reliability of the semi-empirical data can be seen, for example, by the value of ΔE (S_1,S_0) estimated at 298 K for the non-phenolic DBDO analogue: an excitation energy of 4.41 eV (282 nm) was obtained, in good agreement with the maximum peak observed for the absorption spectra of both compounds.

TD-DFT and CIS approaches gave more complete and quantitative information about the electronic structure of the excited states, in good agreement with the experimental data.

Acknowledgements

The authors are grateful to CAPES/COFECUB (Project 422/03). AEHM is very indebted to CNPq (Brazil) for research grants. To Dr. Marcelo H. Gehlen, IQSC/USP, for the cession of infrastructure of his laboratory to perform time-resolved measurements and to Lucas Ferreira de Paula and Renata Faria de Souza for spectroscopic, fluorimetric and HPLC measurements.

References

[1] C. Gardrat, R. Ruggiero, W. Hoareau, A. Nourmamode, S. Grelier, B. Siegmund, A. Castellan, J. Photochem. Photobiol. A Chem. 167 (2004) 111.
[2] P. Karhunen, P. Rummakko, A. Pajunen, G. Brunow, J. Chem. Soc. Perkin Trans. 1 (1996) 2303.
[3] M. Drumond, M. Aoyama, C.L. Chen, D. Robert, J. Wood Chem. Technol. 9 (1989) 421.
[4] M. Erickson, S. Larsson, G.E. Miksche, Acta Chem. Scand. 27 (1973) 127.
[5] C. Gardrat, R. Ruggiero, W. Hoareau, L. Damigo, A. Nourmamode, S. Grelier, A. Castellan, J. Photochem. Photobiol. A Chem. 169 (2004) 259.
[6] D.F. Eaton, Pure Appl. Chem. 60 (1988) 1107.
[7] J.R. Lakowicz, Principles of Fluorescence Spectroscopy, second ed., Kluwer Academic/Plenum, New York, USA, 1999.
[8] B. Valeur, Molecular Fluorescence: Principles and Applications, Wiley-VCH, Weinheim, FRG, 2002.
[9] F. Wilkinson, W.P. Helman, A.B. Ross, J. Phys. Chem. Ref. Data 24 (1995) 663.
[10] AMPAC with Graphical User Interface, Version 8.16.1, Semichem Inc., Shawnee Mission, USA, 2005.
[11] D. McQuarrie, J.D. Simon, Physical Chemistry: A Molecular Approach, University Science Books, California, USA, 1997.
[12] R. Bauernschmitt, R. Ahlrichs, Chem. Phys. Lett. 256 (1996) 454.
[13] M.J. Frisch, G.W. Trucks, H.B. Schlegel, G.E. Scuseria, M.A. Robb, J.R. Cheeseman, J.A. Montgomery Jr., T. Vreven, K.N. Kudin, J.C. Burant, J.M. Millam, S.S. Iyengar, J. Tomasi, V. Barone, B. Mennucci, M. Cossi, G. Scalmani, N. Rega, G.A. Petersson, H. Nakatsuji, M. Hada, M. Ehara, K. Toyota, R. Fukuda, J. Hasegawa, M. Ishida, T. Nakajima, Y. Honda, O. Kitao, H. Nakai, M. Klene, X. Li, J.E. Knox, H.P. Hratchian, J.B. Cross, C. Adamo, J. Jaramillo, R. Gomperts, R.E. Stratmann, O. Yazyev, A.J.Austin, R. Cammi, C. Pomelli, J.W. Ochterski, P.Y. Ayala, K. Morokuma, G.A. Voth, P. Salvador, J.J. Dannenberg, V.G. Zakrzewski, S. Dapprich, A.D. Daniels, M.C. Strain, O. Farkas, D.K. Malick, A.D. Rabuck, K. Raghavachari, J.B. Foresman, J.V. Ortiz, Q. Cui, A.G. Baboul, S. Clifford, J. Cioslowski, B.B. Stefanov, G. Liu, A. Liashenko, P. Piskorz, I. Komaromi, R.L. Martin, D.J. Fox, T. Keith, M.A. Al-Laham, C.Y. Peng, A. Nanayakkara, M. Challacombe, P.M.W. Gill, B. Johnson, W. Chen, M.W., Wong, C. Gonzalez, J.A. Pople, Gaussian 03, Revision B.05, Gaussian Inc., Pittsburgh, PA, 2003.
[14] R.E. Stratmann, G.E. Scuseria, M.J. Frisch, J. Chem. Phys. 109 (1998) 8218.
[15] D. Fengel, G. Wegener, Wood—Chemistry, Ultrastructure, Reactions. Walter De Gruyter, Berlin, Fed. Rep. Germany, 1984.
[16] D.C. Harris, M.D. Bertolucci, Symmetry and Spectroscopy: An Introduction to Vibrational and Electronic Spectroscopy, Dover, New York, USA, 1989.
[17] A. Gilbert, J. Baggott, Essentials of Molecular Photochemistry, Blackwell, London, UK, 1991.
[18] R.M. Silverstein, C.C. Bassler, T.C. Morrill, Spectrometric Identification of Organic Compounds, fifth ed., John Wiley, New York, USA, 1991.
[19] O. Bastiansen, L. Fernholt, B.N. Cyvin, S.J. Cyvin, S. Samdal, A. Almenningen, J. Mol. Struct. 128 (1985) 59.
[20] S. Samdal, O. Bastiansen, J. Mol. Struct. 128 (1985) 115.
[21] R. Bauernschmitt, R. Ahlrichs, J. Chem. Phys. 104 (1996) 9047.
[22] M.E. Casida, C. Jamorski, K.C. Casida, D.R. Salahub, J. Chem. Phys. 108 (1998) 4439.
[23] D.J. Tozer, N.C. Handy, J. Chem. Phys. 109 (1998) 10180.
[24] W. Koch, M.C. Holthausen, A Chemist's Guide to Density Functional Theory, second ed., Wiley-VCH, Weinheim, Fed. Rep. Germany, 2001.
[25] C. Reichardt, Chem. Rev. 94 (1994) 2319.
[26] P. Suppan, J. Photochem. Photobiol. A Chem. 50 (1990) 293.
[27] J. Ribeiro, M.Sc. Dissertation, Universidade Federal de Uberlândia, 2003.
[28] S.L. Murov, I. Carmichael, G.L. Hug, Handbook of Photochemistry, second ed., Marcel Dekker, New York, 1993.
[29] A.E. da Hora Machado, D.E. Nicodem, R. Ruggiero, D.S. Perez, A. Castellan, J. Photochem. Photobiol. A Chem. 138 (2001) 253.

[30] A. Castellan, H. Choudhury, R.S. Davidson, S. Grelier, J. Photochem. Photobiol. A Chem. 81 (1994) 117.
[31] N. Miyoshi, M. Ueda, K. Fuke, Y. Tanimoto, M. Itoh, G. Tomita, Z. Naturforsch, Teil B 37 (1982) 649.
[32] A. Castellan, C. Vanucci, H. Bouas-Laurent, Holzforschung 41 (1987) 231.
[33] D.S. Argyropoulos, in: D.S. Argyropoulos (Ed.), Advances in Lignocellulosics Characterization, Tappi Press, Atlanta, USA, 1999.
[34] W.J. Wehre, J. Yu, P.E. Klunzinger, L. Lou, A Brief Guide to Molecular Mechanics and Quantum Chemical Calculation, Wavefunction Inc., Irvine, USA, 1998.